

<https://doi.org/10.1038/s41612-025-00914-3>

# Global atmospheric distribution of microplastics with evidence of low oceanic emissions

Shanye Yang<sup>1,2,3</sup>, Guy Brasseur<sup>1,4</sup>✉, Stacy Walters<sup>4</sup>, Pablo Lichtig<sup>1</sup> & Cathy W. Y. Li<sup>1</sup>

Recent investigations based on sea–air transfer physical mechanistic studies suggest that the global ocean’s contribution to atmospheric microplastic emissions is significantly lower (four orders of magnitude) than previously estimated. However, no atmospheric models or observations have yet validated this lower emission flux, leaving the analysis without adequate validation and practical significance. Here, we provide quantitative estimates of the global atmospheric microplastic budget based on this reduced oceanic flux. Our model aligns well with observed atmospheric microplastic concentrations and suggests that the ocean functions more as a sink than a source, contributing only ~0.008% of global emissions but accounting for ~15% of total deposition. This challenges the previous view of the ocean as the primary atmospheric microplastic source, urging a reassessment of pollution mitigation strategies.

Plastic, which was invented by Belgian chemist Leo Hendrik Baekeland in 1907, revolutionized the materials industry: it emerged as a superior alternative to metals and biological materials in the interest of resource conservation<sup>1</sup>. However, serious concern has been expressed about the exponential growth in plastic consumption. Since World War II, more than 8300 Tg (million tons) of plastic have been manufactured, with the annual production having increased exponentially from under 2 Tg/year in 1950 to 390 Tg/year in 2021<sup>2,3</sup>. Around 60% of plastics have been discarded in the environment<sup>4</sup>. By 2016, among these plastic pollutants, approximately 6.5–27% consisted of microplastics, defined as plastic particles <5 mm<sup>5</sup>. These tiny particles can enter the atmosphere from aquatic and terrestrial sources, contributing to the global plastics cycle<sup>6</sup>. Since the first observation of microplastics in the atmosphere conducted in 2015<sup>7</sup>, these particles have been detected at various locations, with concentrations decreasing from densely populated to remote areas. Atmospheric microplastics are believed not only to have a potential impact on climate<sup>8</sup> but also pose a threat to the human respiratory and digestive system<sup>9</sup>. Once they enter the bloodstream, they can infiltrate the circulatory system, triggering heart attacks and strokes<sup>10</sup>. Additionally, they can affect other organs through oxidative stress, inflammation, and immune dysfunction. They also alter the biochemical and energy metabolism, impair cell proliferation, and disrupt microbial metabolic pathways. They affect organ development and are a source of carcinogenicity<sup>11</sup>. Therefore, a better understanding of microplastic sources with accurate estimations of atmospheric emission fluxes and global

transport is crucial as a prerequisite for the implementation of monitoring and control measures of microplastic wastes.

Until now, the establishment of emission inventories of microplastics has faced major challenges, mainly due to the large differences (up to 4 orders of magnitude) in the estimation of the fluxes from the ocean<sup>6,12–15</sup>. In 2020, Allen et al. discovered that the ocean emits microplastics in the atmosphere<sup>16</sup>. Initially, model inversions assumed high fluxes from the oceans relative to the continental sources (i.e., road sources and dust sources from agriculture, bare soils, landfills, residential activities, etc.)<sup>6,13,14</sup>. For microplastic particles smaller than 70 μm, Brahney et al. and Evangeliou et al. infer from model inversions global oceanic microplastic emission fluxes of approximately 8.6 and 2.4 Tg/year, respectively<sup>6,13</sup>. These estimates were based on the deposition values measured in remote areas of the western United States, with a relatively wide confidence interval ranging from 0 to 22 Tg/year. According to both studies, more than 93% of global atmospheric microplastics are emitted by the oceans. Considering the same particle size range, Fu et al. formulated a model inversion based on available worldwide observations<sup>14</sup>. This recent study led to considerably lower ocean emissions of the order of ~0.17 Tg/year.

Recently, an increasing number of physical sea–air transfer mechanistic studies inferred that the earlier ocean emissions of microplastics were formerly overestimated. Yang et al. performed an analysis of the microplastic transfer between seawater and air based on laboratory simulations of sea spray aerosol formation<sup>12</sup>. They concluded from a bottom-up calculation

<sup>1</sup>Environmental Modeling Group, Max Planck Institute for Meteorology, Hamburg, Germany. <sup>2</sup>Shanghai Key Laboratory of Atmospheric Particle Pollution and Prevention, Department of Environmental Science and Engineering, Fudan University, 200433 Shanghai, China. <sup>3</sup>Shanghai Institute of Pollution Control and Ecological Security, 200092 Shanghai, China. <sup>4</sup>Atmospheric Chemistry Observations and Modeling Laboratory, National Center for Atmospheric Research, Boulder, CO, 80307, USA. ✉e-mail: [guy.brasseur@mpimet.mpg.de](mailto:guy.brasseur@mpimet.mpg.de)

that the global ocean emissions of microplastic particles smaller than 70  $\mu\text{m}$  amount for only  $\sim 8 \times 10^{-4}$  Tg/year, which is four orders of magnitude lower than the estimates from the first models. Subsequently, a growing amount of bottom-up research studies have revealed that the ability of sea spray to transfer microplastics to the atmosphere was substantially lower than initially estimated. Harb et al.<sup>17</sup> and Shaw et al.<sup>18</sup> reported transfer rates of  $\sim 2 \times 10^{-6}$  Tg/year for microplastic particles with diameters smaller than 10  $\mu\text{m}$  and  $\sim 0.1$  Tg/year for those smaller than 200,000  $\mu\text{m}$ , respectively. Additionally, through the analysis of the maximum potential for sea spray aerosol to carry microplastics, and through theoretical calculations of sea–air transfer mechanisms, Yang et al. constrained the oceanic emission flux of microplastic particles smaller than 70  $\mu\text{m}$  to account for  $< 0.01$  Tg/year<sup>15</sup>. This study compared different reported oceanic emission fluxes and concluded that the estimates by Yang et al. and by Harb et al. (i.e., sub-70  $\mu\text{m}$  microplastic particles sources of  $\sim 8 \times 10^{-4}$  Tg/year and sub-10  $\mu\text{m}$  particles sources of  $\sim 2 \times 10^{-6}$  Tg/year), are consistent with physical mechanisms.

In short, there is a substantial discrepancy between the model inversions and the calculations based on physical mechanisms. However, the results from physical mechanism calculations seem to align more closely with observations of lower ocean emissions of atmospheric microplastics. Therefore, we adopt the low oceanic emission rates as derived in the bottom-up mechanistic approach<sup>12</sup> of Yang et al. to simulate the global distribution of atmospheric concentrations of microplastic particles with our global atmospheric model. We examine the spatial dispersion of microplastics across geographical areas and investigate their distribution at various altitudes. We compare the model concentrations with field observations to validate the low ocean emissions adopted in our modeling study.

## Results

### Global distribution of microplastics in the atmosphere

We use the three-dimensional MOZART-4 model to simulate the global distribution of microplastics and to assess the importance of long-range transport of the particles. We assume the major source of microplastics to be continental emissions ( $\sim 10$  Tg/year) with a relatively insignificant source from the ocean ( $\sim 8 \times 10^{-4}$  Tg/year). These particles are grouped in 6 size

bins with diameters centered at 0.5, 1.5, 5, 10, 35, and 70  $\mu\text{m}$ . The simulations are performed over a 2-year period with the global dynamics representative of the years 2013 and 2014. The smaller particles (0.5–10  $\mu\text{m}$ ) are assumed to be in the form of quasi-spherical debris, while the larger particles (35–70  $\mu\text{m}$ ) are in the form of elongated fibers. This particular model setting is referred to as the base model. Since fibers settle more slowly than spherical particles of an equivalent diameter (defined as the diameter of a sphere having the same volume as a particle with any shape), they are expected to reside longer in the air and are transported over longer distances<sup>19</sup>.

Figure 1a, b show the simulated horizontal distributions of the near-surface mass densities of the total microplastic particles with equivalent diameter ranged from 0.5 to 70  $\mu\text{m}$ . Spatial distributions for each individual size bin are shown in Figs. S1 and S2 of the Supplementary Information. The mass concentration of microplastic particles varies by 3 orders of magnitude across the different geographical regions, ranging from  $\sim 8 \times 10^{-3}$  to 2  $\mu\text{g}/\text{m}^3$ , with the smallest particles (0.5  $\mu\text{m}$ ) being the most numerous and most uniformly distributed. Additionally, the concentrations of microplastics are observed to be higher above the land than above the ocean. Elevated concentrations of microplastic particles are notably present in areas with high populations, including the southeastern United States, the Mediterranean, the Middle East, the Indian peninsula, and southeastern Asia. As shown in Fig. 1a, the highest concentrations of microplastic particles are found near the surface around 30°N latitude, where the population density is highest<sup>20</sup>. A similar result was obtained by Brahney et al.<sup>6</sup>.

The fact that the smallest particles included in the model (diameter  $< 1.5$   $\mu\text{m}$ ) exhibit a more horizontally uniform distribution than the larger particles emphasizes the size dependence of atmospheric dispersion of microplastics. Particles with equivalent diameters ranging between 5 and 10  $\mu\text{m}$  are present primarily over continents and in off-shore regions, while particles within diameters ranging between 35 and 70  $\mu\text{m}$  tend to remain closer to their emission sources (Fig. S2e and f). In other words, as the atmospheric settling velocity of particles (see the “Methods” section) is strongly size-dependent, the large microplastic particles are more rapidly deposited on the surface in the vicinity of their sources, while the smallest particles are more likely to be transported globally.

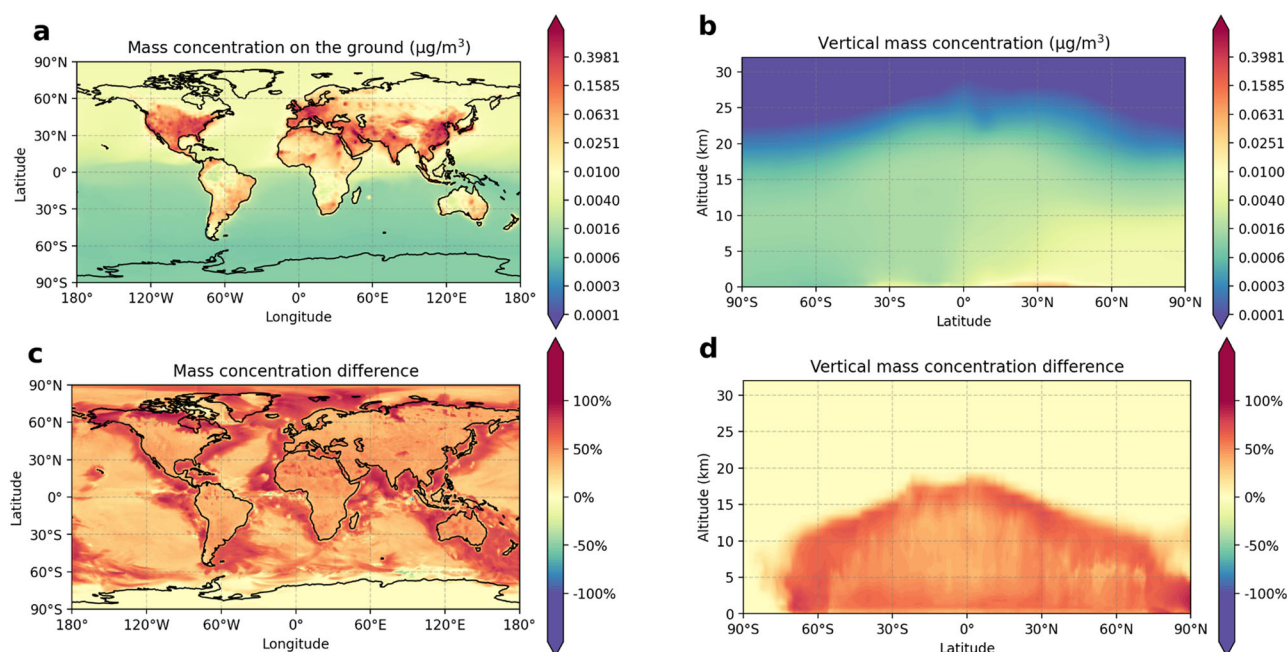


**Fig. 1 | Spatial distribution of the atmospheric concentration of microplastic particles.** **a.** Horizontal distribution (base case) of mass density ( $\mu\text{g}/\text{m}^3$ ) for sub-70  $\mu\text{m}$  microplastic particles in the near-surface layer of the model (altitude of 0–50 km). **b.** Vertical and latitudinal distribution (base case) of zonal mean mass

density for sub-70  $\mu\text{m}$  microplastic particles. Similar plots for each size bin are provided in Figs. S2 and S3. **c.** **d.** Percentage difference in the mass concentrations for particles represented in the base versus the spheres case, for the same conditions as for (a) and (b). The percentage difference is expressed as (base–spheres)/base.

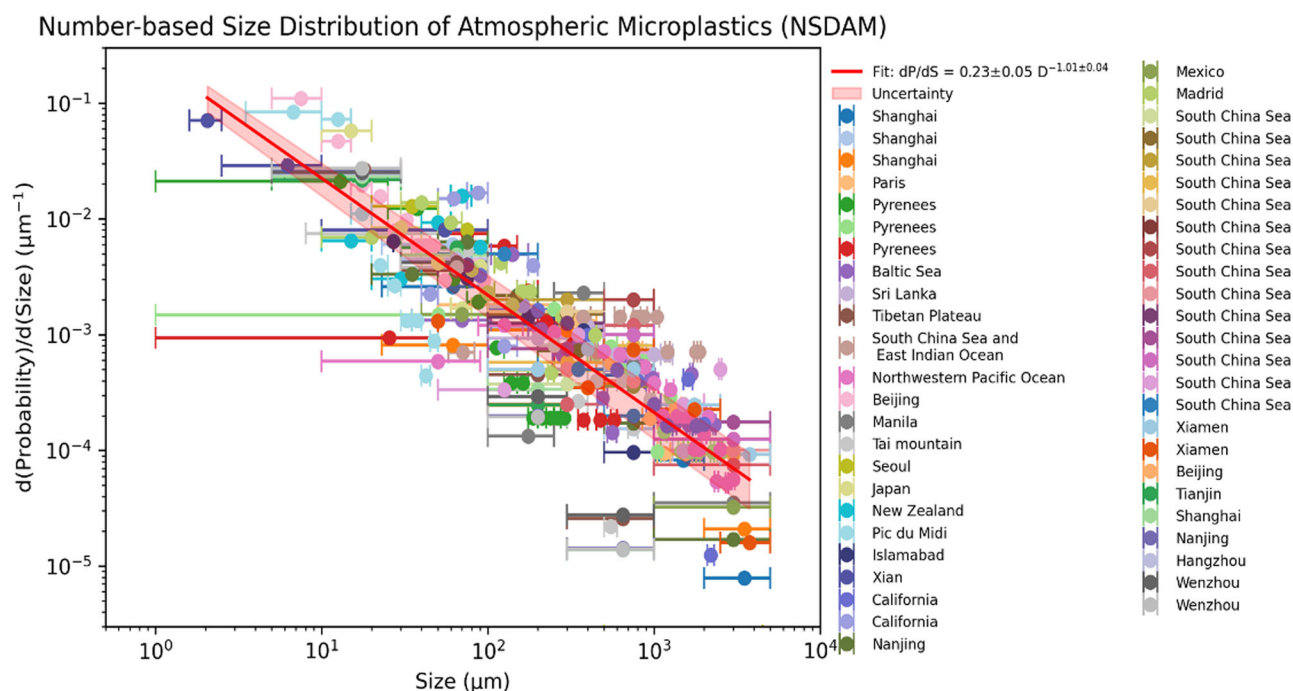


**Fig. 2 | Atmospheric microplastic size distribution probability density.** Values obtained by summarizing the size distribution of atmospheric suspended microplastics across different size bins, as observed at the locations indicated on the right

side of the figure<sup>20–22,24–43</sup>. Each bin is represented by horizontal lines in the figure, with the dots indicating the midpoint of each bin.

Our model also provides a first insight into the vertical dispersion of microplastic particles in the atmosphere (Fig. 1b). In general, microplastic particle concentrations decrease as the altitude increases. Figure S3 shows that, within the altitude range of 0–32 km, microplastic particles with diameters of 0.5–1.5  $\mu\text{m}$  are vertically dispersed more uniformly relative to the larger-size particles, exhibiting higher concentrations at high altitudes. At high altitudes, the concentrations are highest near the equator, with the smaller particles displaying higher mass concentrations compared to larger microplastic particles. Interestingly, a large number of particles with a diameter of 70  $\mu\text{m}$  reach the 15 km altitude. This indicates that even the largest particles are carried to the tropical upper troposphere by strong upwelling motions and convective activity. When accounting for particles with diameters smaller than 70  $\mu\text{m}$ , our model simulations indicate that  $\sim 0.03$  Tg of microplastics are suspended in the atmosphere. The atmospheric burden of microplastics for each of the 0.5–70  $\mu\text{m}$  size bins is provided in Table S3.

Finally, in order to assess the effect of particle shape on the distribution and deposition of microplastics, we performed an additional model simulation in which all particles are assumed to be spherical debris. We refer to this particular model setting as spheres. We show in Fig. 1c and d the differences between the two model cases. When the large particles are represented as fibers rather than spheres, an enhanced number of them are lifted to nearly 20 km altitude and are transported to the ocean, especially to the Arctic region. Yang et al.'s experiment found that fibers are difficult to release from seawater into the atmosphere<sup>12</sup>, yet a significant amount of microplastic fibers have been detected in offshore air<sup>20–22</sup>. Our model shows that the total atmospheric burden of particles is higher, and the number of particles transported from the continents to the oceans is larger when these particles are assumed fibers rather than spheres.

### Atmospheric microplastic size distribution

To properly compare the model results with actual observations, the particle size range (1–5000  $\mu\text{m}$ ) of microplastics provided by our model (0.5–70  $\mu\text{m}$ ) needs to be harmonized with the size ranges of the observed particles. Since different instruments used for these measurements are characterized by

different detection limits of particle sizes, they capture different fractions of the particles' size distribution. For example, detection thresholds of FTIR, Raman, and SEM-EDX instruments, usually in the range 1–100  $\mu\text{m}$ <sup>23</sup>, can be very different. As a result, significant discrepancies exist between the microplastics' number densities measured by these different instruments, even at identical locations. Therefore, the concentrations derived by the model, which cover the particles with a limited size range from 0.5 to 70  $\mu\text{m}$ , cannot be directly compared with the measurements that cover the particles with sizes in the wider range of 1–5000  $\mu\text{m}$ .

Observed atmospheric microplastic abundances are conventionally reported in number densities (number of microplastic particles per cubic meter of air, MP/m<sup>3</sup>). Through examining data reported in the literature for suspended particles<sup>20–22,24–43</sup>, it is found that the number density of the microplastics decreases with the size of the particles following a logarithmic rule. Since the larger particles tend to settle more rapidly than the smaller particles, the size distributions of deposited and suspended particles are different. The size distributions reported here only address suspended microplastics and do not include information on the particles deposited on the surface. We deduce a probability density of microplastic particles for the atmosphere as a function of the size of the particles based on the literature. Most observation sites (28 out of 49) have reported size distributions based on the largest dimension of the microplastic particles, without considering their specific shapes. A relation was derived from the data at the midpoints of each size bin interval to obtain the probability distribution curve<sup>44,45</sup> shown in Fig. 2. The uncertainties of the fitted parameters were derived from the standard errors of the covariance matrix obtained during the nonlinear least-squares fitting process.

With the high correlation ( $R^2 \sim 0.7$ ) found in Fig. 2, the proposed relation provides a good representation of the size distribution for atmospheric microplastics. Since the adopted relation is based on global suspended microplastic data from 49 locations, encompassing varying shapes and including remote, rural, and urban areas, it is possible to estimate the concentrations of microplastics at different sizes from the concentration derived at a specific size interval using this function. This greatly facilitates comparisons between measurements performed worldwide by different

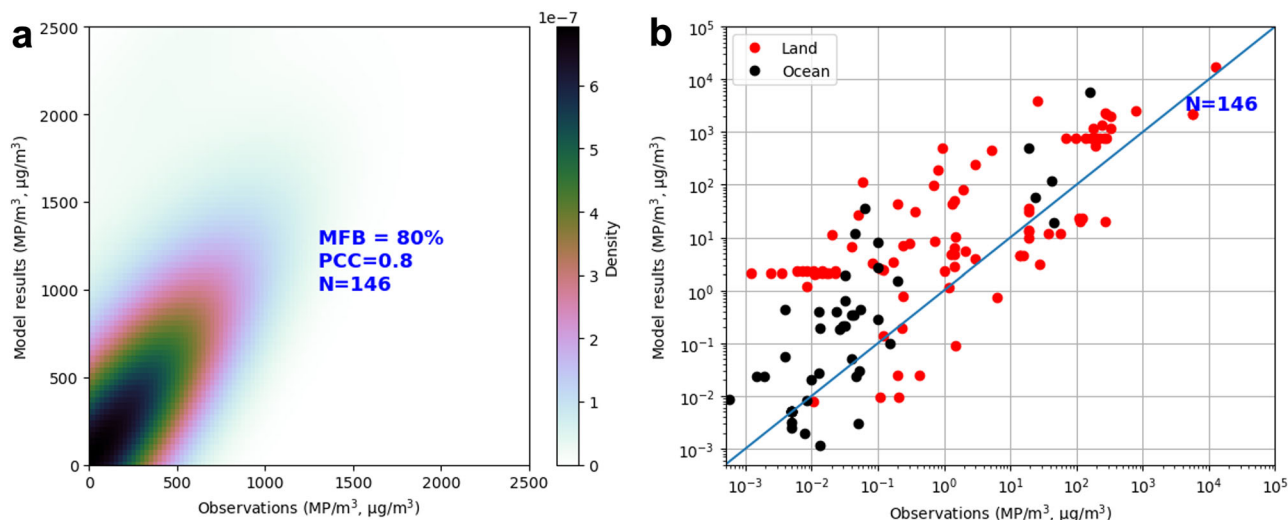
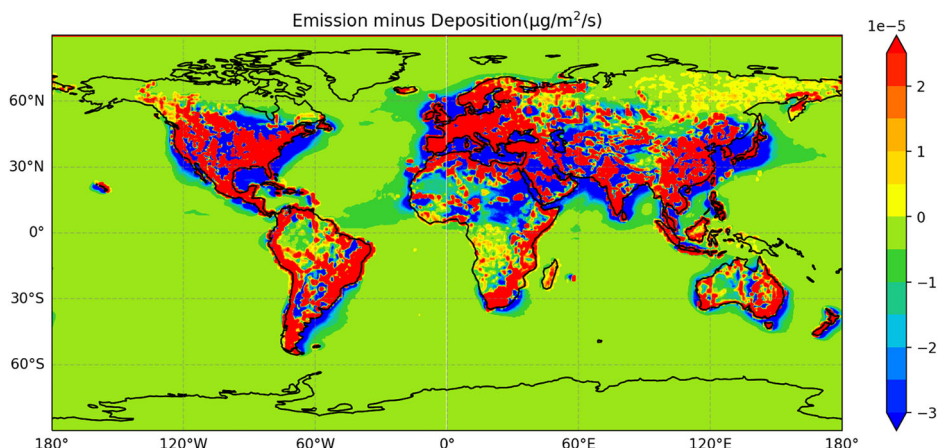


**Fig. 3 | Model versus observed microplastic particle concentrations.** **a** Kernel density estimation. **b** Scatter plot of model versus observation. Modeled concentrations are fitted to the observed size range according to NSDAM. The colored

line represents the line of best fit using an orthogonal regression. The graph refers to 146 data points [MP/m<sup>3</sup> or µg/m<sup>3</sup>]<sup>16,20–22,24–43,46–83</sup>.

**Fig. 4 | Net surface exchange rate of sub-70 µm microplastic particles.** The net exchange rate represents the difference between the surface emission and deposition rates.



devices with varying detection size limits. Here, we refer to this function as the number-based size distribution of atmospheric microplastics (NSDAM). NSDAM is used to extrapolate the calculated concentrations of microplastic particles with the 0.5–70 µm size range to the concentrations of particles observed in all the size ranges covered by the respective instruments. This extrapolation is then used to evaluate our model results.

**Model evaluation**

We evaluate our calculated airborne microplastic number concentrations with available observations. Using this NSDAM, we extrapolate the modeled concentrations of 0.5–70 µm microplastics to the sizes that are detected by the instruments but are not explicitly accounted for by the model<sup>16,20–22,24–43,46–83</sup>. The observations of microplastic particles covering similar size ranges often differ by three orders of magnitude, even if they are conducted in the same city (e.g., Beijing<sup>26,46</sup> and Shanghai<sup>24–26</sup>). Therefore, in our analysis, differences between the observed and modeled data within three orders of magnitude are considered to be acceptable. Our simulations agree surprisingly well with most of the 146 observations, even at an elevation up to 3.5 km<sup>42</sup>. Two point-by-point comparisons between the observations and the modeled values are shown in Fig. 3a. The mean fractional bias (MFB) is 80%, and the Pearson correlation coefficient (PCC) is 0.8 (see Eqs. (3) and (4)), indicating that our model results are consistent

with the reported observations at a large number of sites. Relative to the previously global microplastic models<sup>6,13</sup> by Brahney et al. and Evangeliou et al. the agreement found in our model is enhanced. Fu et al.’s inverse model fit the observations well, even though their concentration data points differ from the observations within three orders of magnitude<sup>14</sup>. However, since their model is based on an inverse approach using observations, it naturally aligns more closely with the observed data. Therefore, in comparison with other studies, our compiled emissions inventory derived from a bottom-up analysis (see the “Methods” section) appears to match observed concentrations relatively well.

**Surface deposition of microplastics**

We now investigate the impact of microplastic pollution at the Earth’s surface in various regions of the world by computing the global distribution of the particle’s deposition rates. The geographical distribution of the deposition rate (expressed here in mass) is shown in Fig. S5. The highest deposition rate occurs in Eastern North America, Europe, and Southeast Asia. More details are provided in Table S1.

The difference between the emission (see geographical distribution in Fig. S6) and deposition rates, which represents the net exchanges (in mass) of microplastics at the surface, is shown in Fig. 4. This figure highlights that, with our assumptions, the continents, and particularly the densely

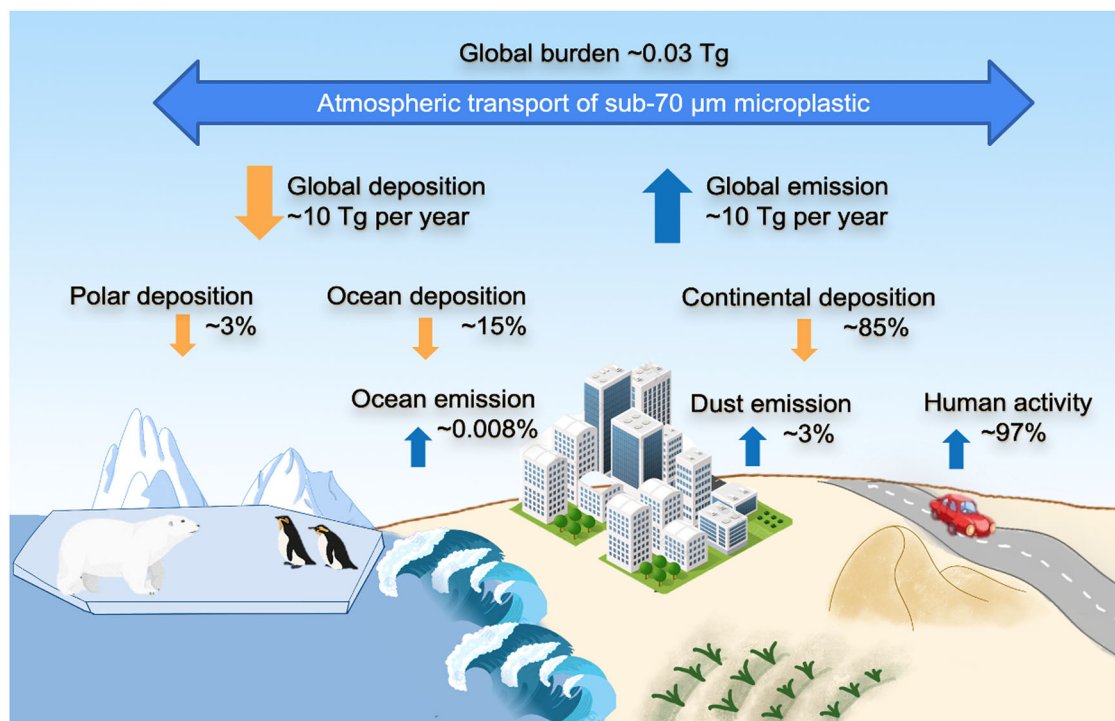


**Fig. 5 | Schematic representation of global surface-atmosphere exchanges of sub-70 µm microplastics particles.** The yellow arrows represent the deposition. The blue arrows represent the emissions.

populated areas, are generally a source of atmospheric microplastics, while the oceans represent a sink. The largest sinks are in the coastal regions since, due to their limited buoyancy, the largest and heaviest microplastic particles predominantly settle in offshore areas. Smaller and lighter particles can be carried to more distant regions. As a result, coastal areas experience a higher rate of microplastic sedimentation compared to open oceans. Furthermore, the oceans in the northern hemisphere are subjected to greater microplastic sedimentation than those in the southern hemisphere.

The deposition of microplastic particles in polar regions represents a growing concern. Our model suggests that  $5 \times 10^{-5}$  and  $8 \times 10^{-8}$  Tg/year of microplastic particles with diameters of 0.5–1.5 and 5–70 µm are deposited on the surface of Antarctica, respectively. In the Arctic ice-covered areas, where the extent of both sea ice and land ice sheet reached its maximum in the year 2002, the deposition of 0.5–1.5 and 5–70 µm microplastic particles amounts to  $9 \times 10^{-4}$  and  $3 \times 10^{-2}$  Tg/year, respectively. The relatively high deposition rate in the Arctic compared to Antarctica is likely due to the proximity of the emission sources (Europe, North America) and to the presence of human settlements in high-latitude regions of the Northern Hemisphere, where direct microplastic emissions occur in significant quantities. In Antarctica, a continent distant from human settlements, only the smallest particles (in the 0.5–1.5 µm range) that are transported over long distances are reaching the area. These results highlight the global impact of microplastic pollution and demonstrate that microplastic emissions have far-reaching effects, especially in the case of the smallest particles. As shown in Fig. 5, ~3% of the total global deposition of sub-70 µm microplastics reaches the polar regions.

#### Global budget and atmospheric residence time of microplastic particles

We summarize our model results by showing in Fig. 5 a schematic with our estimate of the global budget of microplastic particles in the atmosphere. With the assumptions adopted here, the global emission of microplastic particles (~10 Tg/year) is attributed primarily to continental sources, accounting for nearly ~100% of the total emissions. Among this, human

activities contribute to ~97% of the emissions, while dust particles account for ~3%. Ocean emissions represent only ~0.008% of the total flux from the atmosphere into the ocean. About ~85% of microplastics are deposited on the continent and ~15% onto the ocean. The deposition in the polar regions, involving primarily the smallest particles, accounts for ~3%. From the atmospheric burden and emissions estimated for the different size bins of the particles, the atmospheric residence time ranges from 1 year in the case of particles with 0.5 µm diameter to about 1 h for particles with 70 µm diameter. When integrating over size, the mean residence time is close to 6 months for the smallest particles (0.5–1.5 µm) and 2.6 h for the largest particles (5–70 µm).

#### Discussion

In summary, our model simulations based on low oceanic emission flux values<sup>12</sup> provide global distributions of microplastic particles that are consistent with 146 observational data points. They suggest that the role of the ocean sources is low and highlight the importance of long-range transport for particles emitted on the continent. The model, with its emission sources located primarily in densely populated regions, highlights the substantial exposure risks for a large fraction of the human population. Although the ocean contributes only about 0.008% as a source of atmospheric microplastics, it plays a crucial role as a sink, absorbing ~15% of the total atmospheric microplastic deposits.

Regarding the three-dimensional distribution of atmospheric microplastics, 5–70 µm large particles predominantly settle on land and near coastlines, whereas the 0.5–1.5 µm smaller ones are transported over long distances to the open ocean and polar regions, resulting in a more uniform distribution throughout the global atmosphere. With about 10 Tg/year of emissions and deposition per year, the atmospheric burden of the sub-70 µm particles is close to 0.03 Tg. Effective mitigation of microplastic-related risks for human health and ecosystems hinges on a comprehensive understanding of atmospheric microplastic dynamics.

However, with limited experimental data available and the simplifications introduced in our model, we should highlight some limitations in our study:

First, the largest uncertainty in our modeling study arises from insufficient information on emission fluxes. While we adopt for the model simulations the lowest reported oceanic emission fluxes, the continental emissions encompass many sources that are not yet fully quantified, including industrial production, commercial activities, and daily residential activities. Consequently, our estimates of continental emission sources can have significant errors. Despite this uncertainty, our study has demonstrated that low oceanic emission fluxes combined with high continental emission fluxes provide a good fit for global observations. However, the exact range of this uncertainty on emissions cannot yet be rigorously determined, so more work is needed to address this particular problem.

Second, microplastic particles with diameters smaller than 20  $\mu\text{m}$  that are deposited on the surface can be remobilized by strong winds, which provides a source of resuspension, believed to represent <60% of the deposition<sup>84</sup>. In our simulations, we have neglected resuspension since this contribution is smaller than the error associated with the primary emission rates<sup>85</sup>.

Third, in-cloud scavenging contributes to the deposition of microplastics but is significant only for particles with diameters smaller than about 1  $\mu\text{m}$ <sup>86–91</sup>. Besides, as plastic particles are generally hydrophobic and do not easily become cloud condensation nuclei<sup>92</sup>, they were found in very low concentration inside clouds<sup>93</sup>. In-cloud scavenging is therefore ignored in our simulations.

Fourth, it is important to note that the current modeling approach does not account for the chemical and physical aging processes that influence the transport dynamics of microplastics. These aging processes are influenced by factors such as humidity, ultraviolet radiation, secondary aerosol formation, and bacterial activity, among others. The lack of relevant mechanistic studies on microplastic aging limits our ability to accurately incorporate these processes into the models. Therefore, the current modeling results may not fully capture the complete behavior and fate of microplastics in the atmosphere.

## Methods

### Microplastic size distribution

The global size distribution of microplastics in the atmosphere as reported in Fig. 2 is based on observations of atmospheric suspended microplastics from various locations worldwide, is expressed as a probability density function<sup>44,45</sup>.

$$d(\text{Probability})_i = \frac{n_i}{N} \frac{1}{d(\text{Size})_i} \quad (1)$$

where  $d(\text{Probability})_i$  is the probability density of the size interval  $i$  [ $\mu\text{m}^{-1}$ ] and  $n_i$  is the number density of particles in the same interval.  $N$  is the total number density of particles. This function captures the number percentage  $\frac{n_i}{N}$  of microplastics in the atmosphere corresponding to each particle size interval ( $d(\text{Size})_i$ ). Previously reported size distributions are mostly based on the largest dimension of the microplastic particles, without distinguishing between different shapes<sup>21,30–32,34,37,40–43</sup>.

### Model description

The transport and fate of microplastic particles in the atmosphere is simulated by the Model for Ozone and Related Species, version 4 (MOZART-4), an offline global chemical transport model developed at the National Center for Atmospheric Research (NCAR)<sup>94</sup>. In this study, the global model simulations are performed over a period of 2 years with a spatial horizontal resolution of  $0.50^\circ \times 0.63^\circ$ , or  $\sim 50$  km, and with 48 vertical levels. Dynamical forcing by meteorological quantities required to simulate the long-range transport of particles is taken from the GEOS5 Atmospheric Forcing database for the years 2013 and 2014<sup>95</sup>.

The equivalent diameter bins adopted in the model are centered at 0.5, 1.5, 5, 10, 35, and 70  $\mu\text{m}$ . This selection is based on the following reasons: First, suspended particulate matter typically has a diameter of <100  $\mu\text{m}$ <sup>96,97</sup>, and particles smaller than 50  $\mu\text{m}$  are entrained into the boundary layer and

can subsequently be transported over long distances<sup>98</sup>. Therefore, we select particles smaller than 70  $\mu\text{m}$  for global atmospheric transport simulations to cover the main size range of microplastics involved in atmospheric transport. Second, this size range is consistent with the commonly reported size ranges in atmospheric modeling and emission flux studies applied to microplastics<sup>6,12,14</sup>.

The microplastic shapes considered in our model simulations are debris and fibers, which represent the observed particles in more than 90% of the cases<sup>26–28,35,36,39,41,42,56–59,99</sup>. We represent debris as spheres<sup>100,101</sup>. For these particles, the adopted settling velocity follows Stokes' law<sup>86</sup> and is therefore proportional to the square of the particle's diameter. By assuming that the plastic density is close to 1  $\text{g}/\text{cm}^3$ <sup>6</sup>, the resulting velocities derived for each size bin are provided in Table S2. It aligns with the reports by Tatsii et al. regarding the settling velocity of spheres<sup>19</sup>.

Fibers are defined as particles with an aspect ratio larger than 3<sup>37,46</sup>. As the cross-sectional diameter of plastic fibers currently found in the atmosphere is >10  $\mu\text{m}$ <sup>30</sup>, the aspect ratio cannot reach 3 for the particles with equivalent diameters of 0.5, 1.5, 5, and 10  $\mu\text{m}$ . Therefore, we assume that the fiber shape applies only to particles whose equivalent diameters cover the 35 and 70  $\mu\text{m}$  size bins. According to Yuan et al., most fibers have an equivalent diameter in the range of 30–50  $\mu\text{m}$ , while fibers with an equivalent diameter of <20  $\mu\text{m}$  do not exist<sup>56</sup>. Particles tend to settle with their largest projected area normal to the line of motion<sup>102</sup>. Therefore, elongated fibers experience greater drag during settling than agglomerated fragments of equivalent volume<sup>103</sup>. As a result, fibers have a lower settling velocity compared to debris and are transported to larger horizontal distances<sup>104</sup> relative to debris/spheres with an equivalent diameter. For fibers with a 70  $\mu\text{m}$  equivalent diameter, the settling velocity is 3.8–8 cm/s according to Tatsii et al.<sup>19</sup>, and 2–6.1 cm/s according to Xiao et al.<sup>105</sup> For fibers with a 35  $\mu\text{m}$  equivalent diameter, the settling velocity is 1.8–3.6 cm/s according to Xiao et al.<sup>105</sup>. Here, we adopt the midpoint of these ranges for the settling velocity of the fibers, as detailed in Table S2.

Washout (wet scavenging of particles by precipitation) is derived by a simplified (linear) formulation, in which a loss term with a diameter-dependent loss coefficient is added to the conservation equations. This loss coefficient  $\Lambda(D)$  ( $\text{s}^{-1}$ ) is calculated by<sup>87</sup>

$$\Lambda(D) = \alpha a(D) + (1 - \alpha) b(D) \quad (2)$$

where  $0 < \alpha < 1$  represents the ratio between convective to total precipitation rates. Coefficients  $a(D)$  and  $b(D)$  represent the size-dependent scavenging rates for heavy and light precipitation, respectively. Deposition parameters for each particle size bin are listed in Table S2. Rainout (in-cloud scavenging processes by which aerosols act as cloud condensation nuclei) is not explicitly considered in our simulations.

### Surface emissions of microplastics

As mentioned above, we explore here the consequences of assuming a very low contribution of ocean emissions to atmospheric microplastics following the experimental study of Yang et al. The low oceanic emissions calculated through the physical mechanism of particulate emissions, amount to  $8 \times 10^{-4}$  Tg/year (unless specified otherwise, the emission fluxes mentioned below refer to microplastics in a size range of 0–70  $\mu\text{m}$ )<sup>12</sup>.

The considerably larger terrestrial sources include primarily the mobilization of windblown dust and the contribution of human activities. According to the inversion models of Evangelidou et al. and Fu et al. windblown dust emissions are estimated to be 0.1 and 0.11 Tg/year<sup>13,14</sup>, respectively. Based on the recent estimate by Yang et al.<sup>106</sup>, the total soil-to-air particulate emission ranges from 0.0002 to 0.6 Tg/year. Here, we use for this particular category of emissions the midpoint value of this range and we adopt 0.3 Tg/year as the total emission flux.

Emissions resulting directly from human activities are more complex to quantify and include wear and tear of vehicle tires and brakes, agricultural production, industrial production, commercial activities, daily residential

activities, etc.<sup>6,13,14,107</sup>. However, only the emissions from vehicle tires and brakes (0.115 Tg/year<sup>14</sup>, <10 μm of 0.43 Tg/year<sup>88</sup>, and <100 μm of 0.28 Tg/year<sup>13</sup>) and agricultural production (0–0.45 Tg/year<sup>6,13,14</sup>) are available. So far, emissions from industrial production, commercial activities, and daily residential activities have not been quantitatively analyzed, due to the difficulty in separating and analyzing the emissions from these sources. However, it has been established that most of these particles are released in the atmosphere in the form of fibers<sup>26–28,35,36,39,41,42,56–59,99</sup>. Since, according to Yang et al. fibers are not easily emitted through water-to-air transfer<sup>12</sup> and are not produced in significant amounts by agricultural greenhouse film debris or vehicle tire wear and break debris, it is speculated that industrial production, commercial activities and daily residential activities are the major sources of fiber emissions in the atmosphere.

While the contributions of atmospheric sources of the ocean and windblown particles are negligible (~0.3 Tg/year), we assume that the emissions from human activities amount to 10 Tg/year, which is at the upper bound of the total emission estimates from previous studies (0.3–8.6 Tg/year)<sup>6,13,14</sup>.

In summary and based on our analysis and assumptions, oceanic sources, microplastic dust windblow, and emissions from human activities contribute respectively to ~0.008%, ~3%, and ~97% of the total emissions (Fig. 5). Recent studies indicate that airborne microplastic concentrations over land are an order of magnitude higher than those over the oceans. Additionally, airborne microplastic concentrations above roads are twice as high as those in other terrestrial outdoor environments<sup>108</sup>. Combining the emission data (Fig. S6), emission fluxes are particularly high in densely populated areas, with human activities being the dominant source of atmospheric microplastics.

### Mean fractional bias and Pearson correlation coefficient

The mean fractional bias (MFB) and Pearson correlation coefficient (PCC), which are used to assess the model performance, are defined by

$$MFB = \frac{1}{N} \frac{\sum_{i=1}^N (C_m - C_o)}{\sum_{i=1}^N \left( \frac{C_m + C_o}{2} \right)} \times 100\% \quad (3)$$

$$PCC = \frac{\sum_{i=1}^N [(C_o - \underline{C}_o)(C_m - \underline{C}_m)]}{\sum_{i=1}^N [(C_o - \underline{C}_o)^2 (C_m - \underline{C}_m)^2]} \quad (4)$$

where  $C_m$  and  $C_o$  represent modeled and measured quantities and  $N$  is the total number of observations. MFB is a symmetric performance indicator that gives equal weights to under- and over-estimated concentrations (minimum to maximum values range from –200% to 200%)<sup>13</sup>. PCC is a measure of the linear correlation between the modeled and observed datasets<sup>109</sup>. The modeled concentration is derived by combining the concentration from the 6 size bins, and by utilizing the NSDAM relation. This approach ensures that the modeled concentration aligns with the observed data within the same diameter range.

### Data availability

Data in this work is available upon request from the corresponding author.

### Code availability

The codes used to perform the simulations are available upon request from the corresponding author.

Received: 24 April 2024; Accepted: 8 January 2025;

Published online: 28 February 2025

### References

- PAVITT, J. Early plastics: perspectives 1850–1950. *J. Des. Hist.* **11**, 175–177 (1998).
- Plastics Europe. *Plastics—the Facts 2022* (Plastics Europe, 2022).
- Neira, M. The Minderoo–Monaco Commission on Plastics and Human Health. *Ann. Glob. Health* **89**, 22 (2023).
- Geyer, R., Jambeck, J. R. & Law, K. L. Production, use, and fate of all plastics ever made. *Sci. Adv.* **3**, e1700782 (2017).
- Lau, W. W. Y. et al. Evaluating scenarios toward zero plastic pollution. *Science* **369**, 1455–1461 (2020).
- Brahney, J. et al. Constraining the atmospheric limb of the plastic cycle. *Proc. Natl Acad. Sci. USA* **118**, e2020719118 (2021).
- Dris, R. et al. Microplastic contamination in an urban area: a case study in Greater Paris. *Environ. Chem.* **12**, 592–599 (2015).
- Revell, L. E., Kuma, P., Ru, E. C. L., Somerville, W. R. C. & Gaw, S. Direct radiative effects of airborne microplastics. *Nature* **598**, 462–467 (2021).
- Chen, Y., Meng, Y., Liu, G., Huang, X. & Chai, G. Probabilistic estimation of airborne micro- and nanoplastic intake in humans. *Environ. Sci. Technol.* **58**, 9071–9081 (2024).
- Marfella, R. et al. Microplastics and nanoplastics in atheromas and cardiovascular events. *N. Engl. J. Med.* **390**, 900–910 (2024).
- Ali, N. et al. The potential impacts of micro-and-nano plastics on various organ systems in humans. *eBioMedicine* **99**, 104901 (2023).
- Yang, S. et al. Constraining microplastic particle emission flux from the ocean. *Environ. Sci. Technol. Lett.* **9**, 513–519 (2022).
- Evangelidou, N., Tichý, O., Eckhardt, S., Zwaafink, C. G. & Brahney, J. Sources and fate of atmospheric microplastics revealed from inverse and dispersion modelling: from global emissions to deposition. *J. Hazard. Mater.* **432**, 128585 (2022).
- Fu, Y. et al. Modeling atmospheric microplastic cycle by GEOS-Chem: an optimized estimation by a global dataset suggests likely 50 times lower ocean emissions. *One Earth* **6**, 705–714 (2023).
- Yang, S., Lu, X. & Wang, X. A perspective on the controversy over global emission fluxes of microplastics from ocean into the atmosphere. *Environ. Sci. Technol.* <https://doi.org/10.1021/acs.est.4c03182> (2024).
- Allen, S. et al. Examination of the ocean as a source for atmospheric microplastics. *PLoS ONE* **15**, e0232746 (2020).
- Harb, C., Pokhrel, N. & Foroutan, H. Quantification of the emission of atmospheric microplastics and nanoplastics via sea spray. *Environ. Sci. Technol. Lett.* **10**, 513–519 (2023).
- Shaw, D. B., Li, Q., Nunes, J. K. & Deike, L. Ocean emission of microplastic. *PNAS Nexus* **2**, pgad296 (2023).
- Tatsii, D. et al. Shape matters: long-range transport of microplastic fibers in the atmosphere. *Environ. Sci. Technol.* **58**, 671–682 (2024).
- Ferrero, L. et al. Airborne and marine microplastics from an oceanographic survey at the Baltic Sea: an emerging role of air–sea interaction? *Sci. Total Environ.* **824**, 153709 (2022).
- Liu, B. et al. Occurrence of microplastics in the seawater and atmosphere of the South China Sea: pollution patterns and interrelationship. *Sci. Total Environ.* **889**, 164173 (2023).
- Ding, Y. et al. The abundance and characteristics of atmospheric microplastic deposition in the northwestern South China Sea in the fall. *Atmos. Environ.* **253**, 118389 (2021).
- Luo, X., Wang, Z., Yang, L., Gao, T. & Zhang, Y. A review of analytical methods and models used in atmospheric microplastic research. *Sci. Total Environ.* **828**, 154487 (2021).
- Liu, K. et al. Source and potential risk assessment of suspended atmospheric microplastics in Shanghai. *Sci. Total Environ.* **675**, 462–471 (2019).
- Allen, S. et al. Atmospheric transport and deposition of microplastics in a remote mountain catchment. *Nat. Geosci.* **12**, 339 (2019).
- Zhu, X. et al. Airborne microplastic concentrations in five megacities of Northern and Southeast China. *Environ. Sci. Technol.* **55**, 12871–12881 (2021).
- Liao, Z. et al. Airborne microplastics in indoor and outdoor environments of a coastal city in Eastern China. *J. Hazard. Mater.* **417**, 126007 (2021).

28. Perera, K., Ziajahromi, S., Nash, S. B., Manage, P. M. & Leusch, F. D. L. Airborne microplastics in indoor and outdoor environments of a developing country in South Asia: abundance, distribution, morphology, and possible sources. *Environ. Sci. Technol.* **56**, 16676–16685 (2022).
29. Luo, D. et al. Airborne microplastics in urban, rural and wildland environments on the Tibetan plateau. *J. Hazard. Mater.* **465**, 133177 (2024).
30. Wang, X. et al. Atmospheric microplastic over the South China Sea and East Indian Ocean: abundance, distribution and source. *J. Hazard. Mater.* **389**, 121846 (2020).
31. Ding, J. et al. Atmospheric microplastics in the Northwestern Pacific Ocean: distribution, source, and deposition. *Sci. Total Environ.* **829**, 154337 (2022).
32. Romarate, R. A. et al. Breathing plastics in Metro Manila, Philippines: presence of suspended atmospheric microplastics in ambient air. *Environ. Sci. Pollut. Res.* **30**, 53662–53673 (2023).
33. Xu, X. et al. Characterization of microplastics in clouds over Eastern China. *Environ. Sci. Technol. Lett.* **11**, 16–22 (2023).
34. Choi, H. et al. Comparison of microplastic characteristics in the indoor and outdoor air of urban areas of South Korea. *Water Air Soil Pollut.* **233**, 169 (2022).
35. Nagato, E. G. et al. Differences in microplastic degradation in the atmosphere and coastal water environment from two island nations: Japan and New Zealand. *Environ. Pollut.* **333**, 122011 (2023).
36. Allen, S. et al. Evidence of free tropospheric and long-range transport of microplastic at Pic du Midi Observatory. *Nat. Commun.* **12**, 7242 (2021).
37. Din, K. S., Khokhar, M. F., Butt, S. I., Qadir, A. & Younas, F. Exploration of microplastic concentration in indoor and outdoor air samples: morphological, polymeric, and elemental analysis. *Sci. Total Environ.* **908**, 168398 (2024).
38. Liu, Z., Huang, Q., Chen, L., Li, J. & Jia, H. Is the impact of atmospheric microplastics on human health underestimated? Uncertainty in risk assessment: a case study of urban atmosphere in Xi'an, Northwest China. *Sci. Total Environ.* **851**, 158167 (2022).
39. Gaston, E., Woo, M., Steele, C., Sukumaran, S. & Anderson, S. Microplastics differ between indoor and outdoor air masses: insights from multiple microscopy methodologies. *Appl. Spectrosc.* **74**, 1079–1098 (2020).
40. Rao, W., Fan, Y., Li, H., Qian, X. & Liu, T. New insights into the long-term dynamics and deposition-suspension distribution of atmospheric microplastics in an urban area. *J. Hazard. Mater.* **463**, 132860 (2024).
41. Shruti, V. C., Kutralam-Muniasamy, G., Pérez-Guevara, F., Roy, P. D. & Martínez, I. E. Occurrence and characteristics of atmospheric microplastics in Mexico City. *Sci. Total Environ.* **847**, 157601 (2022).
42. González-Pleiter, M. et al. Occurrence and transport of microplastics sampled within and above the planetary boundary layer. *Sci. Total Environ.* **761**, 143213 (2021).
43. Du, R. et al. Unveiling the suspended atmospheric microplastic pollution in a coastal urban landscape. *J. Clean. Prod.* **442**, 141145 (2024).
44. Prather, K. A. et al. Bringing the ocean into the laboratory to probe the chemical complexity of sea spray aerosol. *Proc. Natl Acad. Sci. USA* **110**, 7550–7555 (2013).
45. Jiang, X., Rotily, L., Villermaux, E. & Wang, X. Submicron drops from flapping bursting bubbles. *Proc. Natl Acad. Sci. USA* **119**, e2112924119 (2022).
46. Li, Y. et al. Airborne fiber particles: types, size and concentration observed in Beijing. *Sci. Total Environ.* **705**, 135967 (2020).
47. Akhbarizadeh, R. et al. Suspended fine particulate matter (PM<sub>2.5</sub>), microplastics (MPs), and polycyclic aromatic hydrocarbons (PAHs) in air: their possible relationships and health implications. *Environ. Res.* **192**, 110339 (2021).
48. Gratzl, J., Seifried, T. M., Koyun, A. & Grothe, H. *Characterization of Microplastics Using Fluorescence Spectroscopy and Online Single Particle Fluorescence Measurements* <https://doi.org/10.5194/egusphere-egu22-9512> (2022).
49. Dris, R. et al. A first overview of textile fibers, including microplastics, in indoor and outdoor environments. *Environ. Pollut.* **221**, 453–458 (2017).
50. Levermore, J. M., Smith, T. E. L., Kelly, F. J. & Wright, S. L. Detection of microplastics in ambient particulate matter using Raman spectral imaging and chemometric analysis. *Anal. Chem.* **92**, 8732–8740 (2020).
51. Syafei, A. D., Nurasrin, N. R., Assomadi, A. F. & Boedisantoso, R. Microplastic pollution in the ambient air of Surabaya, Indonesia. *Curr. World Environ.* **14**, 290–298 (2019).
52. Liu, K. et al. Consistent transport of terrestrial microplastics to the ocean through atmosphere. *Environ. Sci. Technol.* **53**, 10612–10619 (2019).
53. Goßmann, I. et al. Occurrence and backtracking of microplastic mass loads including tire wear particles in northern Atlantic air. *Nat. Commun.* **14**, 3707 (2023).
54. Liu, K. et al. Global inventory of atmospheric fibrous microplastics input into the ocean: an implication from the indoor origin. *J. Hazard. Mater.* **400**, 123223 (2020).
55. Trainic, M. et al. Airborne microplastic particles detected in the remote marine atmosphere. *Commun. Earth Environ.* **1**, 64 (2020).
56. Yuan, Z. et al. Vertical distribution and transport of microplastics in the urban atmosphere: new insights from field observations. *Sci. Total Environ.* **895**, 165190 (2023).
57. Chandrakanthan, K., Fraser, M. P. & Herckes, P. Airborne microplastics in a suburban location in the desert southwest: occurrence and identification challenges. *Atmos. Environ.* **298**, 119617 (2023).
58. Yuan, Z. et al. Atmospheric microplastics at a southern China metropolis: occurrence, deposition flux, exposure risk and washout effect of rainfall. *Sci. Total Environ.* **869**, 161839 (2023).
59. Cunningham, E. M. et al. The transport and fate of microplastic fibres in the Antarctic: the role of multiple global processes. *Front. Mar. Sci.* **9**, 1056081 (2022).
60. Hu, T. et al. Emission of airborne microplastics from municipal solid waste transfer stations in downtown. *Sci. Total Environ.* **828**, 154400 (2022).
61. Kernchen, S. et al. Airborne microplastic concentrations and deposition across the Weser River catchment. *Sci. Total Environ.* **818**, 151812 (2022).
62. Chen, E.-Y., Lin, K.-T., Jung, C.-C., Chang, C.-L. & Chen, C.-Y. Characteristics and influencing factors of airborne microplastics in nail salons. *Sci. Total Environ.* **806**, 151472 (2022).
63. Chang, D. Y. et al. First quantification and chemical characterization of atmospheric microplastics observed in Seoul, South Korea. *Environ. Pollut.* **327**, 121481 (2023).
64. Liu, K., Wang, X., Wei, N., Song, Z. & Li, D. Accurate quantification and transport estimation of suspended atmospheric microplastics in megacities: implications for human health. *Environ. Int.* **132**, 105127 (2019).
65. Amato-Lourenço, L. F. et al. Airborne microplastics and SARS-CoV-2 in total suspended particles in the area surrounding the largest medical centre in Latin America. *Environ. Pollut. (Barking, Essex: 1987)* **292**, 118299–118299 (2022).
66. Xie, Y., Li, Y., Feng, Y., Cheng, W. & Wang, Y. Inhalable microplastics prevails in air: exploring the size detection limit. *Environ. Int.* **162**, 107151 (2022).
67. Yoo, H. et al. Novel single-particle analytical technique for inhalable airborne microplastic particles by the combined use of fluorescence microscopy, Raman microspectrometry, and SEM/EDX. *Anal. Chem.* **95**, 8552–8559 (2023).



68. Kyriakouides, G. & Turner, A. Suspended and deposited microplastics in the coastal atmosphere of southwest England. *Chemosphere* **343**, 140258 (2023).
69. Morioka, T., Tanaka, S., Kohama-Inoue, A. & Watanabe, A. The quantification of the airborne plastic particles of 0.43–11 µm: procedure development and application to atmospheric environment. *Chemosphere* **351**, 141131 (2024).
70. Rao, W., Fan, Y., Li, H., Qian, X. & Liu, T. *New Insights into the Long-Term Dynamics and Deposition-Suspension Distribution of Atmospheric Microplastics in an Urban Area* <https://doi.org/10.2139/ssrn.4563525> (2023).
71. Zapata, R., Douglas, P., Chan, K. L. A., Barratt, B. & Wright, S. L. Microplastic emissions via air and compost from an industrial composting facility in England. *Environ. Pollut. Bioavailab.* **36**, 2296046 (2024).
72. Kaushik, A. et al. Identification and physico-chemical characterization of microplastics in marine aerosols over the northeast Arabian Sea. *Sci. Total Environ.* **912**, 168705 (2024).
73. Sarathana, D. & Winijkul, E. Concentrations of airborne microplastics during the dry season at five locations in Bangkok Metropolitan Region, Thailand. *Atmosphere* **14**, 28 (2022).
74. Dehghani, S. & Pardakhti, A. Characterization of microplastics in the atmosphere of megacity Tehran (Iran). *Environ. Sci. Pollut. Res.* **30**, 106026–106037 (2023).
75. Kirchsteiger, B., Materić, D., Happenhofer, F., Holzinger, R. & Kasper-Giebl, A. Fine micro- and nanoplastics particles (PM<sub>2.5</sub>) in urban air and their relation to polycyclic aromatic hydrocarbons. *Atmos. Environ.* **301**, 119670 (2023).
76. Pandey, D., Banerjee, T., Badola, N. & Chauhan, J. S. Evidences of microplastics in aerosols and street dust: a case study of Varanasi City, India. *Environ. Sci. Pollut. Res.* **29**, 82006–82013 (2022).
77. Narmadha, V. V. et al. Assessment of microplastics in roadside suspended dust from urban and rural environment of Nagpur, India. *Int. J. Environ. Res.* **14**, 629–640 (2020).
78. Wang, X. et al. Exponential decrease of airborne microplastics: from megacity to open ocean. *Sci. Total Environ.* **849**, 157702 (2022).
79. Wang, X. et al. Efficient transport of atmospheric microplastics onto the continent via the East Asian summer monsoon. *J. Hazard. Mater.* **414**, 125477 (2021).
80. Chen, Q. et al. Long-range atmospheric transport of microplastics across the southern hemisphere. *Nat. Commun.* **14**, 7898 (2023).
81. Li, C. et al. Enhanced impacts evaluation of Typhoon Sinlaku (2020) on atmospheric microplastics in South China Sea during the East Asian Summer Monsoon. *Sci. Total Environ.* **806**, 150767 (2022).
82. Caracci, E. et al. Micro(nano)plastics in the atmosphere of the Atlantic Ocean. *J. Hazard. Mater.* **450**, 131036 (2023).
83. Goßmann, I. et al. Unraveling the marine microplastic cycle: the first simultaneous data set for air, sea surface microlayer, and underlying water. *Environ. Sci. Technol.* **57**, 16541–16551 (2023).
84. Henry, C., Minier, J.-P. & Brambilla, S. Particle resuspension: challenges and perspectives for future models. *Phys. Rep.* **1007**, 1–98 (2023).
85. Loosmore, G. A. & Hunt, J. R. Dust resuspension without saltation. *J. Geophys. Res. Atmos.* **105**, 20663–20671 (2000).
86. Henzing, J. S., Olivieri, D. J. L. & Velthoven, P. F. Jvan A parameterization of size resolved below cloud scavenging of aerosols by rain. *Atmos. Chem. Phys.* **6**, 3363–3375 (2006).
87. Nieto, P. J. G., García, B. A., Díaz, J. M. F. & Braña, M. A. R. Parametric study of selective removal of atmospheric aerosol by below-cloud scavenging. *Atmos. Environ.* **28**, 2335–2342 (1994).
88. Evangeliou, N. et al. Atmospheric transport is a major pathway of microplastics to remote regions. *Nat. Commun.* **11**, 3381 (2020).
89. Holopainen, E., Kokkola, H., Laakso, A. & Kühn, T. In-cloud scavenging scheme for aerosol modules. *Geosci. Model Dev. Discuss.* **2020**, 1–30 (2020).
90. Guelle, W., Balkanski, Y. J., Schulz, M., Dulac, F. & Monfray, P. Wet deposition in a global size-dependent aerosol transport model: 1. Comparison of a 1 year 210Pb simulation with ground measurements. *J. Geophys. Res. Atmos.* **103**, 11429–11445 (1998).
91. Yang, Y. et al. Stage-resolved in-cloud scavenging of submicron and BC-containing particles: a case study. *Atmos. Environ.* **244**, 117883 (2021).
92. Mundo, R. D., Petrella, A. & Notarnicola, M. Surface and bulk hydrophobic cement composites by tyre rubber addition. *Constr. Build. Mater.* **172**, 176–184 (2018).
93. Wang, Y. et al. Airborne hydrophilic microplastics in cloud water at high altitudes and their role in cloud formation. *Environ. Chem. Lett.* **21**, 3055–3062 (2023).
94. Emmons, L. K. et al. Description and evaluation of the model for ozone and related chemical Tracers, version 4 (MOZART-4). *Geosci. Model Dev.* **3**, 43–67 (2010).
95. Chi-Fan Shih. *GEOS5 Global Atmosphere Forcing Data* (Research Data Archive at the National Center for Atmospheric Research, Computational and Information Systems Laboratory, 2016).
96. Hinds, W. C. et al. *Aerosol Technology Properties, Behavior, and Measurement of Airborne Particles* (John Wiley & Sons Inc., New York, 1999).
97. Murray Wells, R. *Total Suspended Particulates: Review and Analysis; Environmental Protection Technology Series* (U.S. Environmental Protection Agency, Office of Research and Development, Washington, DC, 1976).
98. Mahowald, N. et al. The size distribution of desert dust aerosols and its impact on the Earth system. *Aeolian Res.* **15**, 53–71 (2014).
99. Yuan, Z. et al. Occurrence and human exposure risks of atmospheric microplastics: a review. *Gondwana Res.* **108**, 200–212 (2022).
100. Wang, S. et al. Measurement of density and shape for single black carbon aerosols in a heavily polluted Urban Area. *Aerosol Air Qual. Res.* **21**, 210162 (2021).
101. Wang, S. et al. Online shape and density measurement of single aerosol particles. *J. Aerosol Sci.* **159**, 105880 (2022).
102. Goral, K. D. et al. Settling velocity of microplastic particles having regular and irregular shapes. *Environ. Res.* **228**, 115783 (2023).
103. Dittmar, S., Ruhl, A. S., Altmann, K. & Jekel, M. Settling velocities of small microplastic fragments and fibers. *Environ. Sci. Technol.* **58**, 6359–6369 (2024).
104. Preston, C. A., Neuman, C. L. M. & Aherne, J. Effects of shape and size on microplastic atmospheric settling velocity. *Environ. Sci. Technol.* **57**, 11937–11947 (2023).
105. Xiao, S., Cui, Y., Brahney, J., Mahowald, N. M. & Li, Q. Long-distance atmospheric transport of microplastic fibres influenced by their shapes. *Nat. Geosci.* **16**, 863–870 (2023).
106. Yang, S. et al. Constraining global emission of microplastics from soil–air interface. *Environ. Sci. Technol. Lett.* **11**, 1207–1213 (2024).
107. Gupta, S. et al. Atmospheric microplastics: perspectives on origin, abundances, ecological and health risks. *Environ. Sci. Pollut. Res.* **30**, 107435–107464 (2023).
108. O'Brien, S. et al. There's something in the air: a review of sources, prevalence and behaviour of microplastics in the atmosphere. *Sci. Total Environ.* **874**, 162193 (2023).
109. Ivatt, P. D. & Evans, M. J. Improving the prediction of an atmospheric chemistry transport model using gradient boosted regression trees. *Atmos. Chem. Phys. Discuss.* 1–33 <https://doi.org/10.5194/acp-2019-753> (2019).

## Acknowledgements

The National Center for Atmospheric Research is sponsored by the US National Science Foundation. The support provided by the China Scholarship Council during the visit of Shanye Yang to Germany is acknowledged. The model simulations have been performed on the

supercomputer of the German Climate Computer Center (Deutsches Klimarechenzentrum, DKRZ) in Hamburg, Germany.

### Author contributions

Guy Brasseur provided comprehensive guidance on the paper. Shanye Yang defined the scientific questions, searched for information, analyzed the results of the model simulations. She conceived and wrote the paper together with Guy Brasseur and Cathy W.Y. Li. Stacy Walters performed the model simulations using the MOZART-4 model. Pablo Lichtig contributed to the analysis of the model results. Cathy W.Y. Li contributed to the compilation of the emission datasets. All authors contributed to the final version of this manuscript.

### Funding

Open Access funding enabled and organized by Projekt DEAL.

### Competing interests

The authors declare no competing interests.

### Additional information

**Supplementary information** The online version contains supplementary material available at <https://doi.org/10.1038/s41612-025-00914-3>.

**Correspondence** and requests for materials should be addressed to Guy Brasseur.

**Reprints and permissions information** is available at <http://www.nature.com/reprints>

**Publisher's note** Springer Nature remains neutral with regard to jurisdictional claims in published maps and institutional affiliations.

**Open Access** This article is licensed under a Creative Commons Attribution 4.0 International License, which permits use, sharing, adaptation, distribution and reproduction in any medium or format, as long as you give appropriate credit to the original author(s) and the source, provide a link to the Creative Commons licence, and indicate if changes were made. The images or other third party material in this article are included in the article's Creative Commons licence, unless indicated otherwise in a credit line to the material. If material is not included in the article's Creative Commons licence and your intended use is not permitted by statutory regulation or exceeds the permitted use, you will need to obtain permission directly from the copyright holder. To view a copy of this licence, visit <http://creativecommons.org/licenses/by/4.0/>.

© The Author(s) 2025